Nanotechnology and Precision Engineering 1 (2018) 226–235

Contents lists available at ScienceDirect

Nanotechnology and Precision Engineering

journal homepage: http://www.keaipublishing.com/en/journals/nanotechnology-and-precision-engineering/

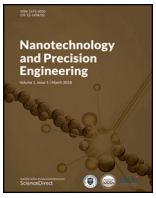

CFD-based design and analysis of air-bearing-supported paint spray spindle

Ali Khaghani *, Kai Cheng

College of Engineering, Design and Physical Sciences, Brunel University London, Uxbridge UB8 3PH, UK

ARTICLE INFO

Keywords:
Air-bearing
CFD analysis
Paint spray spindle
Air-turbine design
Turbine blade design and optimization

ABSTRACT

In this paper, an analytical scientific approach is presented for the design and analysis of an air-turbine-driven paint spray spindle, and it is used to improve further the design concept of the existing spindle applied in automotive coating and paint spraying applications. The current spindle on the market can operate at a maximum speed of 100,000 rpm and features a maximum bell size of 70 mm diameter. Given the increasing demands for high automotive coating/painting quality and productivity in assembly, the design and development of a paint spray spindle with a speed of 145,000 rpm or higher is needed. Computational fluid dynamics (CFD)-based simulation is applied in the approach. Accordingly, CFD simulation-based design and analysis are undertaken, covering the characteristic factors of velocity, pressure of the air supply, rotational speed of the air-turbine, and torque and force reaction on the turbine blades. Furthermore, the turbine blade geometric shape is investigated through the simulations. Three geometrical concepts have been investigated against the original model. The results on Concept_03 verified the higher angular velocity speeds against the theoretical model. The pressure and velocity effects in the blades have been investigated. The results show that the pressure and velocity of the air supply driving the turbine are critical factors influencing the stability of turbine spinning. The results also demonstrate that the force acting on the blades is at the highest level when the adjacent face changes from a straight surface into a curve. Finally, changing the geometrical shape in the turbine likely increases the tangential air pressure at the blades surface and relatively increases the magnitude of the lateral torque and force in the spindle. Notwithstanding this condition, the analytical values surpass the theoretical target values.

1. Introduction

The impact of precision manufacturing is increasingly realized by manufacturing companies. They consider this variable in both long-term and short-term strategies due to the growing demand for high-precision products, machinery, and components and their applications in dental healthcare, automotive and aerospace manufacturing, and consumer goods. The creation of a high-speed spindle is required for the air-bearing system development. Hybrid air journal bearings are widely used in precision engineering applications due to their compelling advantages, such as high motion accuracy, extended maintenance servicing, and frictionless surface contact.[1,2] Moreover, a significant advantage can be gained for hybrid air bearings with ultra-high speed requirements at 100,000 rpm and beyond.[3] Air-bearing-supported spindles provide high rotational speed that can exceed 250 krpm with high accuracy in the printed circuit boarded (PCB) drilling industry. High-precision machining is appropriate with air-bearing spindles. An ultra-precision aerostatic spindle is adopted to enable higher accuracy in precision machining in terms of higher running accuracy, higher operation speeds, and excellent thermal stability when compared with other types of bearings. An aerostatic bearing can avoid the wear thermal error, bearing failure, and additional lubrication system, thereby qualifying as an anti-friction bearing.[4] In the field of fluid mechanics, the design of an air-turbine-driven high-speed paint spindle and air bearing is aimed at achieving the highest operation speed, where the air surface linear speed is an essential design functionality. Overall, however, several issues of concern include the load carrying capacity, which interacts with the paint fluid supply and the bearing parts. Other matters that need to be considered are fluid flow efficiency, tool behavior, and the geometry of the design. To address these issues, a scientific approach is proposed to bridge the gaps between fluid flow, geometrical design, and their interactions with the components and identification of the key factors involved. Moreover, the new design process is essentially required for the optimization and improvement of the products and their implementations.[5,6]

Substantial research, both experimentally and theoretically, has been published over the last decade; they studied the characteristics and performance of air-bearing-supported applications, including the

* Corresponding author.
E-mail addresses: ali.khaghani@brunel.ac.uk (A. Khaghani), kai.cheng@brunel.ac.uk (K. Cheng).

https://doi.org/10.1016/j.npe.2018.12.004

air-driven paint spray spindle. Domnick et al.[7] demonstrated a comparison methodology between a computational fluid dynamics (CFD)-based and experimental study for a rotary bell atomizer paint spray, with direct charging for a rotational speed range of 30,000–60,000 rpm. They observed that droplet charging exerts a direct effect on the bell edges. Domnick[8] also studied the effect of bell geometry on high-speed bell atomization in the automotive industry based on the Newtonian clear coating liquid with three different bell geometries. The conclusion was that with a smoother surface bell, the film disintegration will shorten the length of the paint film at higher bell speeds. Guettler et al.[9] investigated a numerical CFD-based on rotary bell atomization for a high-quality paint spray with a maximum rotational speed of 60,000 rpm, and the results showed that such sprays for automotive coating require significant axial shaping air velocity. Song et al.[10] investigated the effect of a hybrid air journal bearing by solving the Reynolds equation. The examination of the performance and accuracy of the air bearing was based on a study of a high-speed spindle with a maximum rotational speed of 150,000 rpm. The conclusion was made based on the comparison of the CFD simulation and experimental results, where the findings revealed that the effect of rotational speed on the discharge coefficients increases in the upstream inlet and decreases in the downstream one.

From a geometrical design point of view, several patents have been published in this area. Schmitt[11] invented an air-driven turbine spindle, with the blades of the apparatus located in the radial face of the spindle and geometrically possessing a wedge-shaped tapered turbine blade side. The blades are specially designed to maintain a rapid rotational velocity. Herre et al.[12] developed a similar device, and a new blade shape was designed to increase the performance of rotational speed, with a range of 15,000 rpm to 80,000 rpm being achieved. Kutnjak et al.[13] described a new radial turbine apparatus, where the blade shape is designed in association with a blade channel that could prevent the air brake in the inward direction at the exit flow passage. The cross-sectional area of the driven air nozzle is widened in the flow direction of the turbine blades. Brett et al.[14] designed and developed a new rotary atomiser drive spindle. The turbine blades were located axially in the spindle, and at least one gas supply channel was designed for turbine driving. The blade shape was a ring type. A radial nozzle was included to direct gas flow toward the blades, which are defined as adjacent pairs and comprise an outlet with a cross-sectional area of the gas passage. Two turbine exhausts are provided in this design for cooling purposes due to their high rotational speed.

This paper presents an active investigation and analysis on an existing model of an air-driven paint spray spindle with a maximum rotational speed of 100,000 rpm and bell size of 70 mm, with the rotational speed increased to 145,000 rpm. The study is executed by employing a three-dimensional CFD-based methodology while investigating the performance and efficiency of the paint spraying process in the automotive sector. A new concept design is also utilized to investigate the influence of geometry on the blades, pressure, and velocity of the air journal passage, axial effect of force, and torque on a loaded and unloaded paint spray air-driven axial-impulse rotary turbine.

2. Design and analysis of the paint spray atomizer

2.1. Air-turbine-driven rotary atomizer spindle

Classically, an air-driven rotary atomizer spindle is a device that was designed as an application of atomization, which transpires through high-speed rotations of a hollow shaft. Such devices are frequently used to spray materials in tiny forms onto an object material from a source to a bell atomizer for the material and directs the atomized material at the painting target. The air turbine in the paint spray atomizer can be classified as an impulse type, where the source gas impinges onto the blades, causing them to rotate from the rotational axis.

In an axial-flow turbine, gas/liquid flows parallel to the machine axes and enters in the axial direction, pushing the blades in a tangential path. Fig. 1 shows the principle diagram of the air turbine. As shown in the diagram, when the air flow strikes from the inclined nozzle to the blade, the pressure decreases, and the velocity increases. The potential energy of the gas/air will be converted into kinetic energy, whereas the lateral force/torque will be distributed alongside the blade surface. High air pressure and velocity are observed at the nozzle when the air flow is released. However, as the kinetic energy of the gas/air is consumed by the blade tangential surfaces, the velocity will simultaneously decrease at the exit point. The velocity triangle shows that the nozzle angle vector ***V*** plays a key role in the effectiveness of the lateral load ***U*** and the magnitude of the force ***W***.

The rotating atomizer drive spindle comprises a shaft that carries a turbine and a body that includes one or more air conduits to supply an external air flow through the turbine for rotary purposes. The rotary action drives the shaft corresponding to the central axis of the assembly body. The turbine is a structure comprising a ring or disc-shaped rotary body section with multiple blades extruded from the flat surface from one of the sides. The blades are similar in both shape and dimension.[14]

2.2. Governing equation and fluid model

In a high-speed spindle, the air is regarded as perfect gas, and the flow is thus turbulent. The turbulence can be determined as K-ε, where K is the kinetic energy, and ε is the turbulent eddy dissipation. The total heat transfer model is considered, as the kinetic energy effects bear significance in the model. The boundary conditions were applied and explained below.

Continuity equation is defined by the following:

$$\frac{\partial \rho}{\partial_t} + \frac{\partial\left(\rho U_j\right)}{\partial_{Xj}} = 0 \tag{1}$$

Momentum equation is as follows:

$$\frac{\partial \rho U_i}{\partial_t} + \frac{\partial\left(\rho U_i U_j\right)}{\partial_{Xj}} = -\frac{\partial p}{\partial_{Xi}} + \frac{\partial}{\partial_{Xj}}\left[\mu_{\text{eff}}\left(\frac{\partial U_i}{\partial_{Xj}} + \frac{\partial U_j}{\partial_{Xi}}\right)\right] \tag{2}$$

where ρ denotes the density, U_i is the Cartesian velocity component, p represents the pressure, x_i refers to the coordinate axe, and μ_{eff} is the effective viscosity.

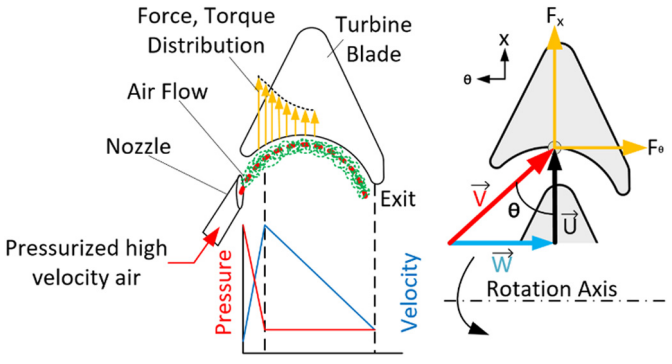

Fig. 1. Air-turbine flow and axial-impulse diagram.

μ_{eff} can be defined as follows:

$$\mu_{\text{eff}} = \mu + \mu t; \mu t = C_{\text{u}\rho}\frac{K^2}{\varepsilon} \tag{3}$$

where μt specifies the eddy viscosity, μ is the molecular dynamic viscosity, C_u is a constant equal to 0.09, K corresponds to the turbulence kinetic energy, and ε is the turbulence eddy dissipation.

The turbulence model is given by:

$$\frac{\partial \rho K}{\partial_t} + \frac{\partial\left(\rho U_j K\right)}{\partial_{Xj}} - \frac{\partial}{\partial_{Xj}}\left(\frac{\mu_{\text{eff}}}{\sigma_k}\frac{\partial K}{\partial_{Xi}}\right) = \mu t\frac{\partial U_i}{\partial_{Xj}}\left(\frac{\partial U_i}{\partial_{Xj}} + \frac{\partial U_j}{\partial_{Xi}}\right) - \frac{2\partial U_i}{3\partial_{Xj}}\left(\frac{\partial U_j}{\partial_{Xj}} + \rho K\right) - \rho\varepsilon \tag{4}$$

$$\frac{\partial \rho \varepsilon}{\partial_t} + \frac{\partial\left(\rho U_j \varepsilon\right)}{\partial_{Xj}} - \frac{\partial}{\partial_{Xj}}\left(\frac{\mu_{\text{eff}}}{\sigma_\varepsilon}\frac{\partial \varepsilon}{\partial_{Xi}}\right) = \frac{\varepsilon}{K}(C_{\varepsilon 1}(\mu t\frac{\partial U_i}{\partial_{Xj}}\left(\frac{\partial U_i}{\partial_{Xj}} + \frac{\partial U_j}{\partial_{Xi}}\right) - \frac{2\partial U_i}{3\partial_{Xj}}\left(\frac{\partial U_j}{\partial_{Xj}} + \rho K\right)) - C_{\varepsilon 2}\rho\varepsilon) \tag{5}$$

where σ_k and σ_ε are the K-ε turbulence model constants and are equal to 1.0 and 1.3, respectively, $C_{\varepsilon 1}$ and $C_{\varepsilon 2}$ are equal to 1.45 and 1.92, respectively.

The energy equation can be defined as follows:

$$\frac{\partial(\rho U_i h_{\text{tot}})}{\partial_{Xj}} = \frac{\partial\left(\lambda\left(\frac{\partial T}{\partial_{xj}}\right)\right)}{\partial_{Xj}} + S_E \tag{6}$$

where, T is the temperature of the fluid, λ is the thermal conductivity, S_E is the source term, which represents the work done by the viscous and pressure forces, h_{tot} is defined as the specific total enthalpy, which is a general case of variable properties, given in terms of the specific static enthalpy, h, and computed as follows:

$$h_{\text{tot}} = h + \frac{1}{2}U^2; h = h(p, T) \tag{7}$$

$$p = \rho RT \tag{8}$$

where U is the velocity magnitude, and R is the gas constant. Eq(8) is the equation for an ideal gas state.[15]

The pressure coefficient is computed as follows:

$$\text{pressure coefficient} = \frac{P_{max} - P_{min}}{P_{\text{inlet}}} \tag{9}$$

where P_{max} denotes the maximum pressure exerted by air on the rotor, P_{min} refers to the minimum pressure exerted by air on the rotor, and P_{inlet} is the air pressure at the inlet. The maximum and minimum pressure exerted by air can be obtained by CFX-Post.[15]

Table 1 illustrates the appropriate theoretical calculations for the loaded and unloaded models. The driving force and torque are the most critical investigation parameters in the simulation for this research.

The Naiver Stokes equation governs the air bearing used in this spindle design. By simplifying this governing equation, mass flow rate is obtained as follows:

$$\dot{m} = \frac{ah^3\left(p_1{}^2 - p_2{}^2\right)}{24\eta RT_1} = \boldsymbol{\rho\nu A} \tag{10}$$

where a is length, that is 0.074 m, h represents the height of the air-bearing film between the bearing and the shaft and is equal to 0.00001143 m, p_1 is the pressure at the inlet of the air bearing (5 ± 0.5 bar), p_2 refers to the pressure at the exhaust of the bearing (1 bar), η corresponds to the air viscosity at 293 K = 0.0000183 Pa/s, R is a constant (3.31 J/mol), T_1 specifies the air-bearing operational temperature (293 K), A is the cross-sectional area of the bearing film, ρ is the air density (1.2041 kg/m^3), and ν is the velocity. Hence, the fluid flow in the air bearing is turbulent.

In addition, the air bearing may experience failure due to vibrations and thermal expansion of the shaft. When the turbine is rotating at high speeds, the shaft will vibrate at specific frequencies, and although the air film is considered to be a frictionless medium of lubrication, in reality, a friction with air molecules persists and may result in thermal expansion of the shaft.

2.3. Geometric design of the paint spray spindle

For this project, the existing model data of a paint spray atomizer air-driven spindle are drawn upon for research and design optimization. The proposed method, using CFD techniques, is employed to investigate and identify the characteristic issues and perform the problem-solving for the model geometrically. As illustrated in Fig. 2(a), the air-driven atomizer spindle consists of a bell, spindle body, bearing, shaft, spacer, thrust plate, and back cap. The spindle includes two air supply inlets, which are separated by 180 degrees from each other, to drive the turbine machined on the front of the back cap. The high-pressurized air supply flows through the inlet passing through the channel into the volume control chamber, as shown in Fig. 2(b), and through a nozzle inclined at an angle from the face of the bearing. The volume control chamber and nozzle are machined on the bearing part item No.2 as shown in Fig. 2(a).

The air supply then exits the nozzle and flows through the pathway in between the adjacent blades, subsequently exiting the spindle by passing through the six exhaust air slots of the thrust plate and finally exiting the spindle entirely through the three exhaust air slots placed on the back cap. The flow of air supply past the blade sections will induce a torque on the turbine shaft, causing it to spin or rotate at specified speeds. As shown in Fig. 2(b), at the same time, paint flows through the hollow part of the turbine shaft as it rotates at high speeds. The paint itself is atomized as it passes through the shaft and the bell and exits the bell as atomized charged paint particles. This condition allows the paint to adhere to the spot as a uniform layer of paint with a

Table 1
Theoretical calculation and comparison between loaded and unloaded models.

Models		Mass, m, (kg)	Angular velocity, ω (1/s)	Velocity, v (m/s)	Kinetic energy (J)	Work input (W)	Horse power (hp)	Force, F (N)	Torque, τ (N•m)
Original model	Unloaded	0.2677	10,471.9	258.95	8,975.3	14,958.85	20.34	42.95	1.062
100,000 rpm	Loaded	0.3607	10,471.9	258.95	12,074.58	20,124.3	27.36	59.87	1.430
New model	Unloaded	0.2677	15,184.36	376.42	18,419.96	30,699.93	41.74	62.99	1.511
145,000 rpm	Loaded	0.3607	15,184.36	376.42	25,504.56	42,507.6	57.79	87.21	2.090

smooth surface. This process will provide the turbine shaft with a thin layer of air, approximately 3–5 μm, that acts as a lubricant, as the shaft is proposed to rotate at high speeds. Other exhaust holes are also machined on most of the air-bearing part.

The exhausts not only operate as an air dumping channel but also cool down the shaft as it rotates at high velocities. According to the data provided, the model developed in this project works at an angular velocity of 100,000 rpm with the bell attached (loading condition), and the paint delivery rate measured is currently at 0.5 L/min. When the shaft rotates at speeds below 45,000 rpm, the paint flowing through the shaft will fail to atomize. However, when the bell is unattached, the maximum rotational speed that the current

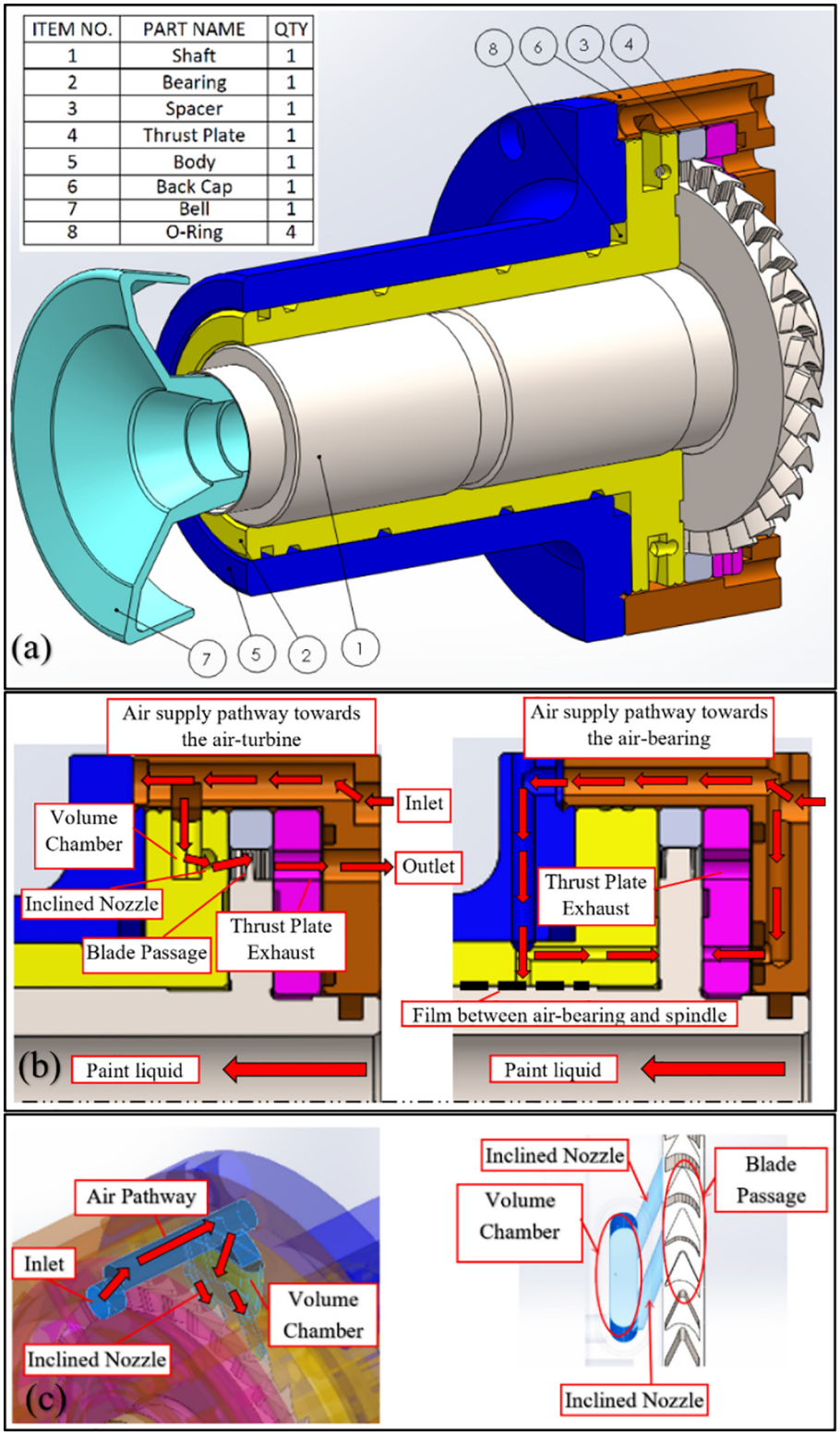

Fig. 2. (a) Assembly of the current air-driven atomizer spindle; (b) Fluid passage channel toward the air-turbine and air-bearing; (c) Volume control chamber and inclined air flow nozzle.

design can achieve approximates 100,000 rpm. Hence, a higher rotary speed can ensure and increase the paint delivery rate, and the capability of the rotary in high rotational speeds under the loaded condition should be investigated. An approximate increase in rotational speed of up to 145,000 rpm and paint delivery of 0.6 L/min or more are the initial targets. In this paper, three different geometrical concept designs are modeled, and their influence on the design is investigated.

3. CFD simulation

The fluid section is exported from the assembly and created as a part using the CAD software Solidworks, whereas the model is simulated using the CFD software available in ANSYS Fluent/CFX, R17. The objective is to simulate the interaction between the rigid body (represented by the spindle blades) and the fluid volume that builds up in the surrounding area. Fig. 3 illustrates the inlet domains of the three concepts considering different geometries. As illustrated in Fig. 3(d), the fluid from the source supply is inserted through the inlet, entering the volume control chamber and then exiting through the outlet.

The velocity of the fluid will presumably increase as it moves out of the nozzle and heads toward the turbine blade. The interaction between the fluid and the passage between adjacent blades will result in the formation of pressure differentiation and forces acting on the turbine blade, leading to the rotational velocity of the turbine about its axial direction. The rigid body is enveloped by a fluid volume, which is air, at a static temperature of 25 °C. The blades in the real position are part of the shaft spindle and are kept floating by an air bearing.

The spindle blade (rigid body or wall), which is the pattern in the fluid section, is given the initial rotational speed of 0 rpm and set as a wall, prompting turbulence in the air flow. Given the variety of the fluid domain, the subdomain, mesh motion of the domain, and numerous other boundary conditions must be defined. The fluid domain is extracted from the 3D CAD assembly design and imported into the simulation model to extricate the torque and force values. The outlet of the fluid model is recognized to be an opening that is subjected to an atmospheric pressure of approximately 1 bar, and the fluid domain is considered to be in a static state throughout the simulation.

The blade section is assumed to be a rotational wall rotating at 0 rpm. Thus, the force and torque in the turbine axial direction can be possibly obtained. The air flow throughout the fluid domain is considered to be a steady-state flow when considering the near-wall parameters. Based on a previous simulation carried out by Min,[15] a rotational speed of 100,000 rpm was achieved. In this research, the investigation is carried out based on several approaches, including changing the geometry of the blades, modification of the angle of the inclined nozzle, and changing the geometry of the cross-sectional area of the inclined nozzle. Nevertheless, to obtain a rotational velocity of 145,000 rpm or higher, the torque forces acting on the turbine blades still need to be higher compared with the previous results.

In this study, three types of geometrical concept designs are obtained. Fig.4 illustrates the geometrical designs in terms of comparison between the original model (a) and the new concept design. Concept_01 in Fig. 4(b) is modified as a straight direction inlet without any brake fluid pathway, whereas Concept_02 in Fig. 4(c) includes a narrowing fluid pathway before the volume chamber. Concept_03 in Fig. 4(d) features a new geometrical design in the turbine blade. The turbine is formed as an axial-impulse turbine, and its rotational speed is completely reliant on the governed geometry shape of the turbine blade. Notwithstanding such condition, the distance between the consecutive blade arrangements and the number of blades should be kept the same as the original model. The modifications are undertaken by adding the curve on the adjacent face of the blade and filleting the sharp edge. Table 2 shows the CFD modeling setup and boundary conditions.

4. CFD result and discussion

The simulation results are obtained via the CFD Post, with a comparison made in terms of the fluid domain behavior between the original model and the concepts.

4.1. Effect of the pressure distribution

From the results, the pressure spreads throughout the fluid domain of the spindle shaft. This finding implies the significantly high pressure that enters through the nozzle. However, the pressure decreases

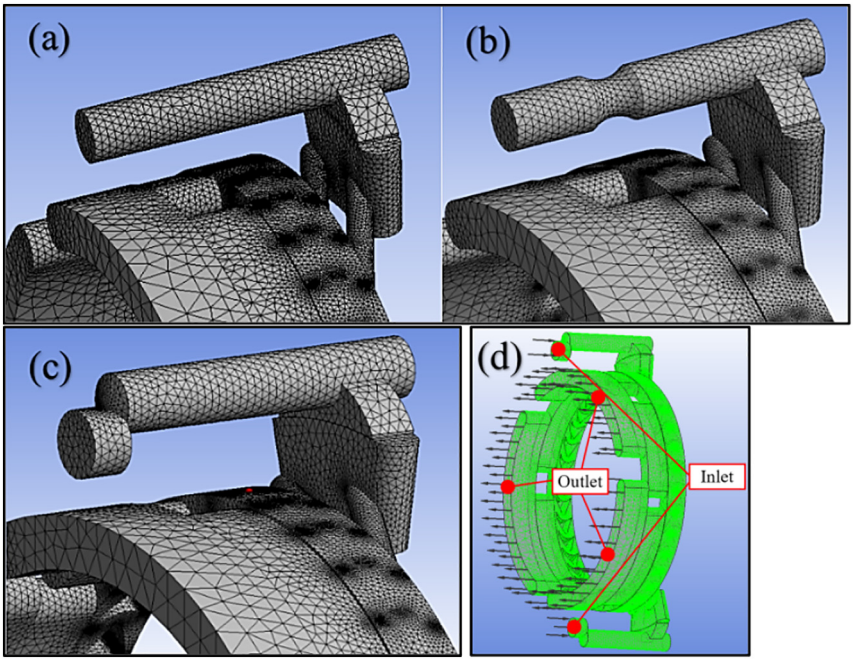

Fig. 3. CFD geometry shape meshing. (a) Concept_01, (b) Concept_02, (c) Concept_03, and (d) Inlet and outlet fluid domains.

steadily as it enters the volume control chamber and exits through the inclined nozzles. The pressurized air travels at the highest speed when it exits the inclined nozzle and hence, strikes immediately the surface of the turbine blade. As discussed in previous section, owing to an instantaneous increase in the pressure, the surfaces where the air hits the blade are aligned with the nozzle blades.

The front curved surface and the straight side of the blade are the most effective areas. The air is less effective and stagnant in the back surface of the blade. High pressure values and kinetic energy conversions are observed at the effective surfaces on the blade. Fig. 5 illustrates the observed pressure distribution in the fluid domains for the original and concept models. As observed from the models, Concept_01 and Concept_02 yield the highest pressure values, which are significantly higher when compared with that of the original model. This result is due to the geometrical modification of the fluid direction made in the fluid pathway channel before the volume control chamber. This abnormality can cause the whole model to function in a highly vibrant and unstable status.

The performance for Concept_03 shows a rational result compared with that of the original model, given that the effective pressure

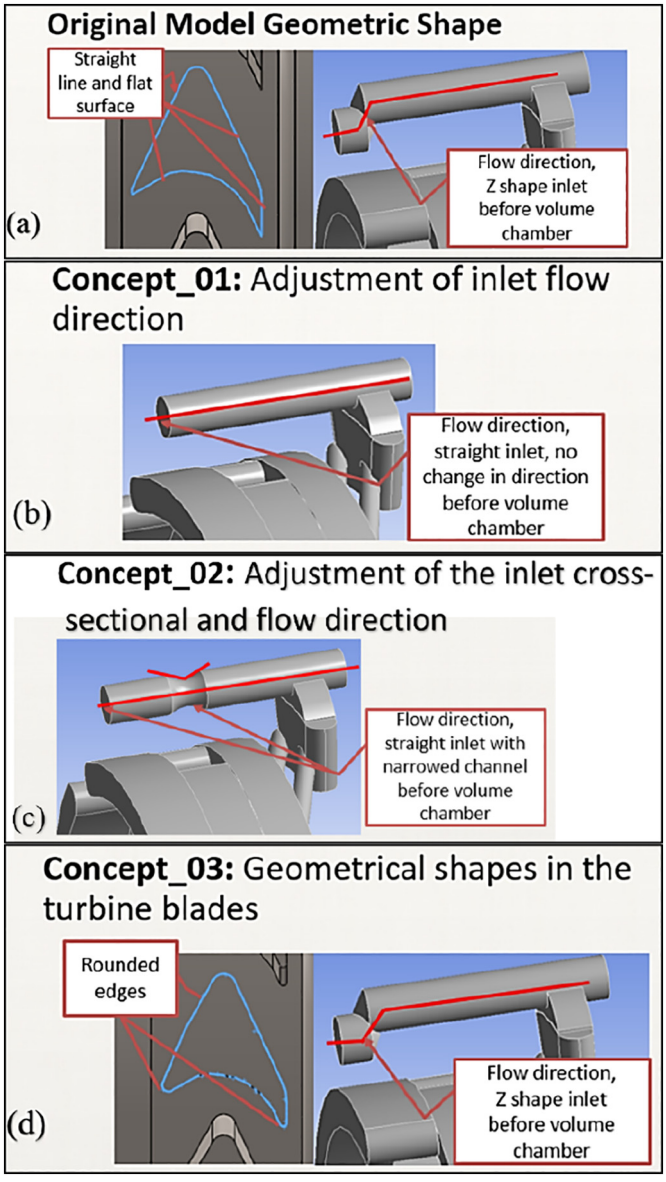

Fig. 4. Fluid domain (a) Original model, (b) Concept_01, (c) Concept_02, and (d) Concept_03.

increases very steadily. As shown in Fig. 6, the pressure distribution is triggered in local coordination at the positions of blades 01, 02, and 03, which are aligned with the inclined nozzle outlet from the volume control chamber.

As illustrated in Fig. 6(a), blades 01 and 03 are aligned with the inclined nozzle, whereas blade 02 is located in the middle. However, for more accurate results, the average pressure value is considered. In such a case, blade 02 features an average tangential pressure distribution with steady-state performance and functionality.

4.2. Effect of the velocity vector

The results obtained from the CFD demonstrate that the pressure spreads throughout the fluid domain of the spindle shaft. The pressure is high as it enters through the inlet, decreases steadily as it enters the volume control chamber, and exits through the inclined nozzles toward the blades and turbine spindle. The fluid passage from this point toward the blades should exhibit a steady-state behavior in terms of velocity. As discussed in the previous section, the pressure distribution is abnormally high in Concept_01 and Concept_02, and this finding is caused by the modification of the geometrical design along the direction of the fluid pathway channel before the volume control chamber. The same scenario can be observed for the fluid velocity vectors in the whole domain region of the FE model.

As shown in Fig.7, the highest velocity value in the global coordination is triggered in Concept_01 and Concept_02. Despite the enhanced the velocity owing to the geometrical design of these particular models, an unbalanced condition will occur in the turbine blade and ultimately result in the spindle functioning in an unstable and uncertain state. Concept_03 shows a more acceptable streamline velocity value when compared with the original model. Fig. 8 shows the local average velocity value that is believed to be located on blade 02, where the most resolute state of the blade functionality should be encountered. The average velocity indicated in blade 02 for Concept_03 shows the optimal value when compared with the original model and other concepts.

4.3. Driving torque and force influence

Extracting the data from the FEM models proves that the kinematic forces created from the fluid energy significantly influence the spindle performance. The generated data from CFX-Post for force and torque on the blades and overall domain, particularly in the X-axis, show that geometrical modification of the shape of blades in Concept_03 influences the tangential forces on the blade surfaces. This result is due the provision of more torque in the spindle axial direction.

The moments of inertia that the turbine shaft maintains as the influencing parameters are involved in the simulations except for the

Table 2
CFD modeling setup and boundary conditions.

CFD modeling setup	Boundary condition
Analysis type	Steady state
Domain type	Fluid domain
Domain material	Air at 25 °C
Reference pressure	1 atm
Morphology	Continuous fluid
Domain motion	Stationary
Heat transfer	Isothermal
Turbulence	K-epsilon, 5% intensity
Wall function	Scalable
Initial condition	Velocity type, cartesian
Velocity component	Automatic
Inlet	Subsonic, 5 bar
Flow direction	Normal to boundary condition
Outlet	Subsonic, 1 bar
Wall	No slip wall, smooth wall roughness
Solver	Upwind, high resolution, 5 s physical timescale, RMS, Global dynamic control

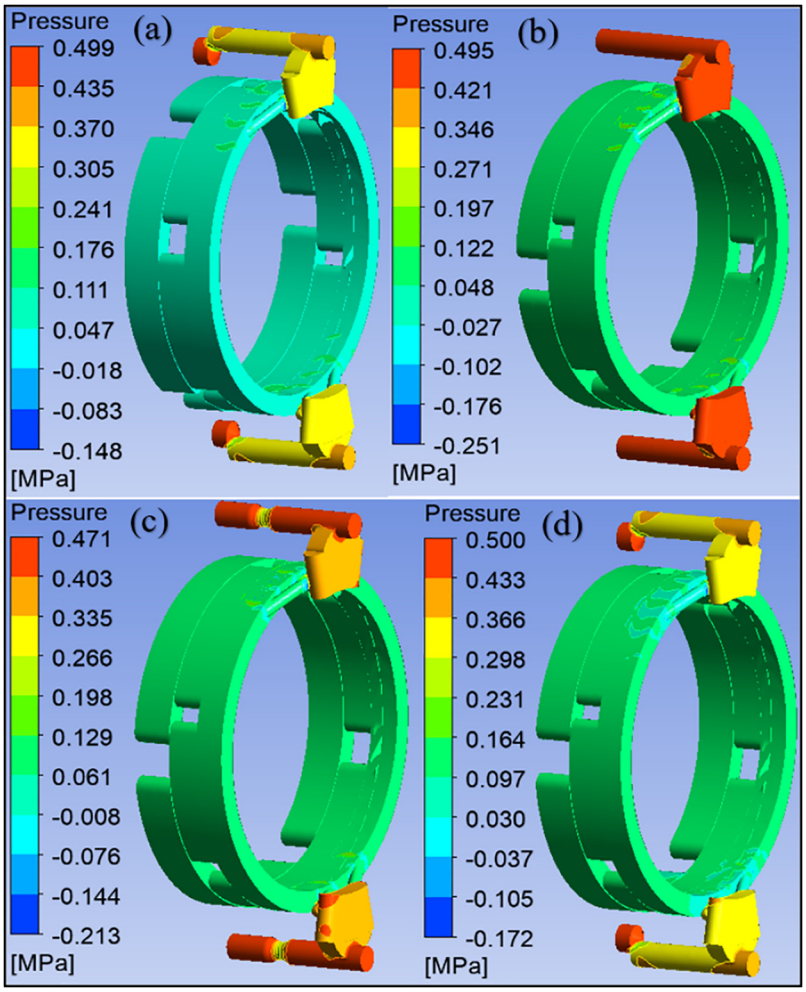

Fig. 5. Pressure distribution through the whole model based on global coordination. (a) Original model, (b) Concept_01, (c) Concept_02, and (d) Concept_03.

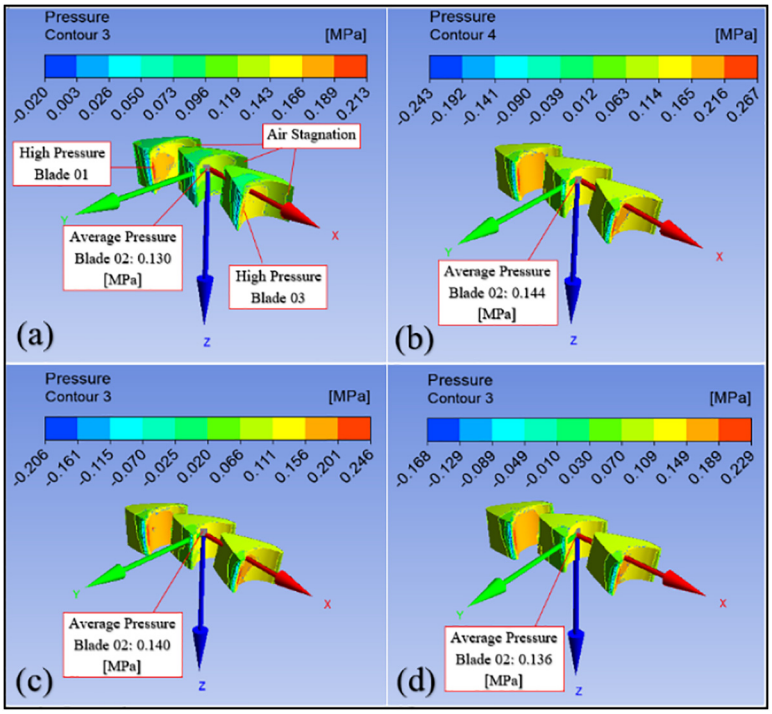

Fig. 6. Pressure distribution based on local coordination; resultant vector of blades 01, 02, and 03. (a) Original model, (b) Concept_01, (c) Concept_02, and (d) Concept_03.

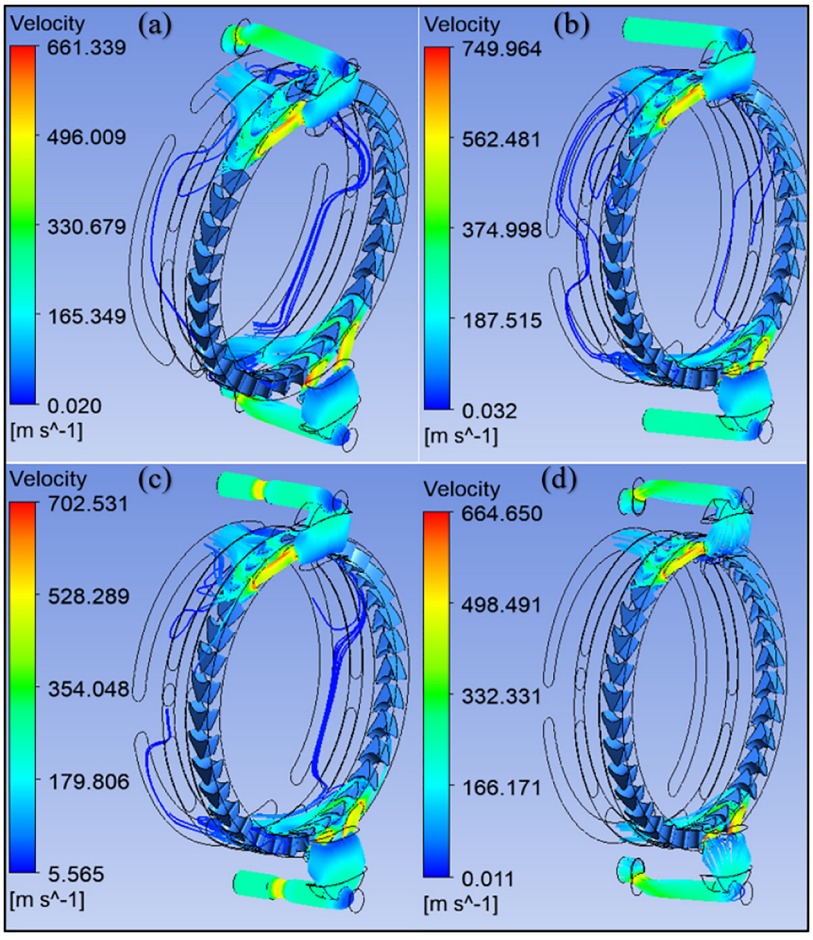

Fig. 7. Velocity vectors. (a) Original model, (b) Concept_01, (c) Concept_02, and (d) Concept_03.

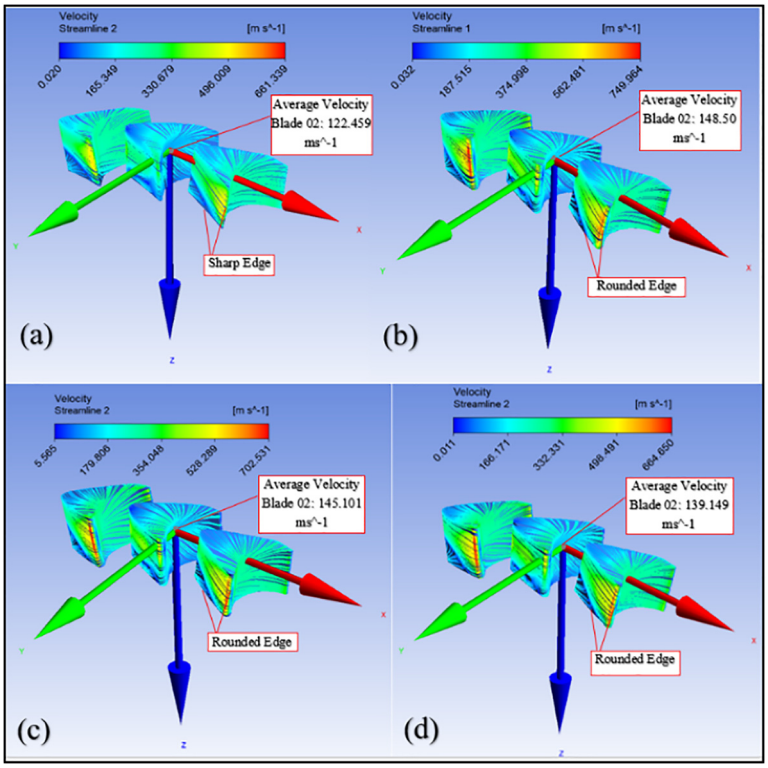

Fig. 8. Velocity vectors based on local coordination; resultant vector of blades 01, 02, and 03. (a) Original model, (b) Concept_01, (c) Concept_02, and (d) Concept_03.

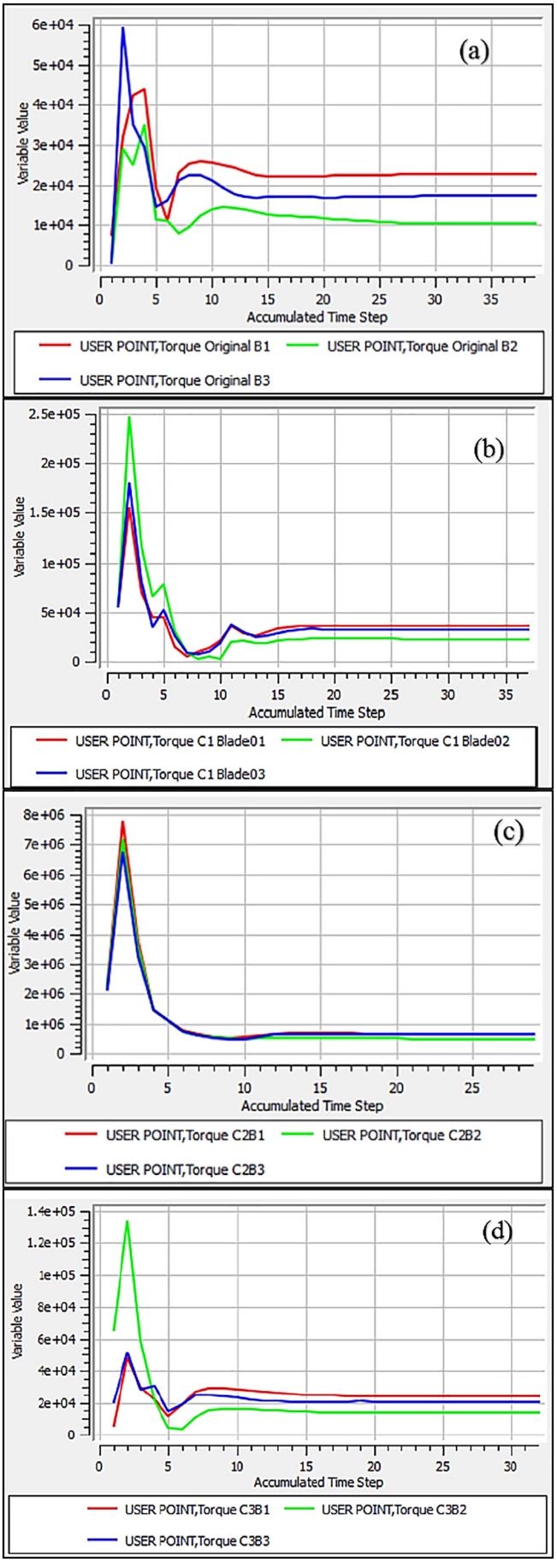

Fig. 9. Global (axial) torque comparison of the blades between the original and three proposed concepts.

forces from the paint itself, which will oppose the swirling effects from a rotational shaft. The torque ratio calculated in the spindle is within the target torque value for the unloaded condition of 145,000 rpm and is evaluated as 1.511 N·m for the turbine based on a rotational speed of 145,000 rpm. Concept_03 shows the best torque and force values. However, Concept_01 and Concept_02 are neglected given their inconsistent performances. Fig. 9 illustrates the unidimensional torque value extracted from CFD versus the accumulated time step. Fig. 9(d) shows that the highest torque value affects the surface body of blade 1 in Concept_03.

In this particular geometry, the CFD results prove that the original model and Concept_03 are almost functioning in a steady state, whereas Concept_01 and Concept_02 are in an unstable condition. However, from the geometrical point of view, a small modification in the geometry of the blades in the original model features a significant and direct effect on the spindle speed and performance. Fig. 10 shows a comparison of the torque generated in the blades between the original model and the new Concept_03 FEM model.

4.4. Result comparison between the theoretical and CFD models

The CFD results must be compared with the theoretical calculation for final proof and validation. The functional torque calculator has been employed in ANSYS CFD Post to generate the actual value of the torque in the blades for all of the concepts in the simulation. Table 3 illustrates the total force and torque calculated in the blades and compares the values between the theoretical calculation described above and the CFD results from the FEM models of the original, Concept_01, Concept_02, and Concept_03. As emphasized in the previous section, the total force and torque slightly increase with Concept_03, with the value approximating 1.76 N·m, which is higher than the calculated value in the theoretical model (1.5 N·m).

For optimum understanding, Fig. 11 shows the scatter data curve that illustrates how total torque and force increase, whereas the trend exponentially ascends based on the geometrical shape and design.

5. Conclusions

• The pressure and velocity of the air supply driving the turbine are critical factors influencing the stability of turbine spinning. Importantly, the paint distribution rate and atomization are entirely reliant on the angular velocity of the turbine. In the first stage of simulation, the results show that changing the geometrical shape in the turbine possibly increases the tangential air pressure at the blade surface and relatively increases the magnitude of the lateral torque and force in the spindle. Notwithstanding such condition, the experimental values surpass the theoretical target values.

- The geometrical design and modification before the volume control chamber show enhancement of the velocity and pressure in the blades. However, this event significantly unbalances the model, leading to unsteady functioning.
- The adjustments in the geometries of turbine blades will result in changes in the driving forces acting on these blades.
- The force acting on the blades is at the highest level when the adjacent face changes from a straight surface into a curve.
- The blade shape is amended, and further modifications are made. Regarding the adjustments to the blade geometry, the results reveal that the turbine generates the highest pressure and gradually increases the torque value, far exceeding the theoretical value needed for the turbine to rotate at 145,000 rpm.

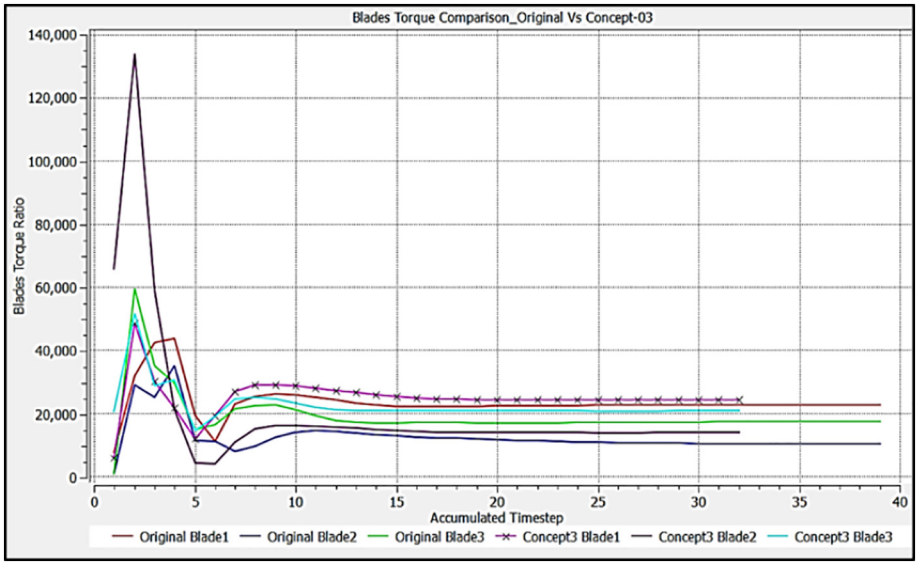

Fig. 10. Torque comparison of the blades of Concept_03 and the original model.

Table 3
Theoretical calculation and CFD result comparison of the torque/force under the unloaded condition.

Item	Simulation CFD result comparison for 145,000 rpm spindle speed under unloaded condition				
	Theoretical	Original	Concept_ 01	Concept_ 02	Concept_ 03
Total force (N)	62	65	61	62	66
Torque (N·m)	1.5	1.7	1.6	1.6	1.76

Future research will concentrate on the investigation of the driving force and torque measurement at the atomizer for the final design verification. Simulation with the transition method and contact interface between the stationary and rotary components is highly recommended. Furthermore, extensive research is required to investigate the paint rate under the loaded condition with the effect of vibrations and thermal factors under high rotational speeds.

Acknowledgement

The authors thank for the PhD Scholarship Support at Brunel University London and the engineering data provided by Loadpoint Bearings Ltd.

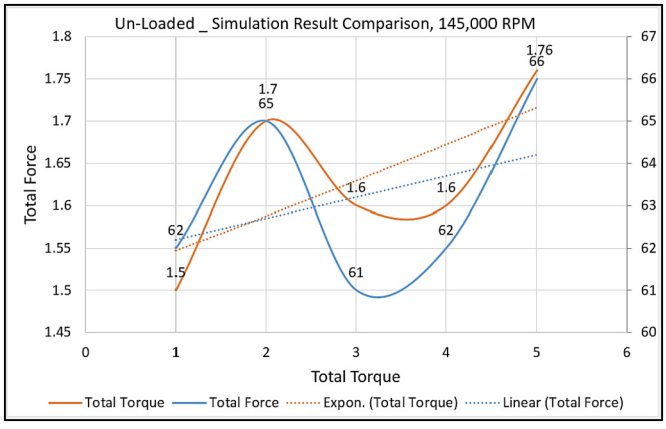

Fig. 11. Comparison of final results according to the torque and force in the spindle under the unloaded condition.

References

1. Cheng K, Rowe WB. Selection strategy for the design of externally pressurized journal bearings. Tribol Int 1995;28(7):465-74.
2. Abele E, Altintas Y, Brecher C. Machine tool spindle units. CIRP Ann Manuf Technol 2010;59(2):781-802.
3. Jia C, Pang H, Ma W, et al. Dynamic stability prediction of spherical spiral groove hybrid gas bearings rotor system. J Tribol 2016;139(2), 021701.
4. Sharma MK, Priyank G. Study of dynamic characteristics and design analysis of bush & spindle of ultra-precision aerostatic bearing. International Journal of Science and Research 2015;4(3):747-52.
5. Akafuah NK. Automotive paint spray characterization and visualization. In: Toda K, Salazar A, Saito K, eds. Automotive Painting Technology: A Monozukuri-Hitozukuri Perspective. Dordrecht: Springer Netherlands; 2013. p. 121-65.
6. Lefebvre AH, VG McDonell. *Atomization and Sprays.* CRC Press. 2017.
7. Domnick J, Scheibe A, Ye Q. The simulation of electrostatic spray painting process with high-speed rotary bell atomizers. Part II: External charging. Part Part Syst Charact 2007;23(5):408-16.
8. Domnick J. Effect of bell geometry in high-speed rotary bell atomization. ILASS-Europe 2010. Brno, Czech Republic: 23rd Annual Conference on Liquid Atomization and Spray Systems; 2010. p. 1-7.
9. Guettler N, Paustian S, Ye Q, et al. *Numerical and Experimental Investigations on Rotary Bell Atomizers with Predominant Air Flow Rates.* Conf Liq At Spray Syst.. 2017
10. Song L, Cheng K, Ding H, et al. Analysis on discharge coefficients in FEM modeling of hybrid air journal bearings and experimental validation. Tribol Int 2018;119:549-58.
11. Schmitt B. Turbine wheel for high speed rotary tools. EP1443181B1; 2004.
12. Herre F, Baumann M, Nolte H, et al. Rotary atomizer turbine and rotary atomizer. EP1388372B1; 2004.
13. Kutnjak J, Krumma H, Beyl T. Rotary atomizer turbine. US20170368561A1; 20-Jan-2015.
14. Brett NE, Graham C, Chris R. Rotary atomiser drive spindles. US 7967552 B2; 2011.
15. Jeh Min NG. *Air Driven Spray Spindle. MSc Dissertation.* London: Brunel University London. 2013.